Size and Shape Effects on the Compressive Strength of High Strength Concrete

J.R. del Viso, J.R. Carmona & G. Ruiz,
E.T.S. de Ingenieros de Caminos, Canales y Puertos, Universidad de Castilla-La Mancha

ABSTRACT: In this paper we investigate the influence of the shape and of the size of the specimens on the compressive strength of high strength concrete. We use cylinders and cubes of different sizes for performing stable stress-strain tests. The tests were performed at a single axial strain rate, 10^{-6} s^{-1}. This value was kept constant throughout the experimental program. Our results show that the post-peak behavior of the cubes is milder than that of the cylinders, which results in a strong energy consumption after the peak. This is consistent with the observation of the crack pattern: the extent of micro-cracking throughout the specimen is denser in the cubes than in the cylinders. Indeed, a main inclined fracture surface is nucleated in cylinders, whereas in cubes we find that lateral sides get spalled and that there is a dense columnar cracking in the bulk of the specimen. Finally, we investigate the relationship between the compressive strength given by both types of specimen for several specimen sizes.

1 INTRODUCTION

By far the most common test carried out on concrete is the compressive strength test. The main reason to understand this fact is that this kind of test is easy and relatively inexpensive to carry out (Mindess et al., 2003). Testing Standard requirements use different geometries of specimens to determine the compressive concrete strength, f_c. The most used geometries are cylinders with a slenderness equal to two and cubes. Shape effect on compression strength has been widely studied and different relationships between compression strength obtained for these geometries have been proposed, mainly from a technological standpoint. Such approach eludes the fact that there is a direct relation between the nucleation and propagation of fracture processes and the failure of the specimen. Indeed, experimental observations confirm that a localized micro-cracked area develops at peak stress (Shah and Sankar, 1987) or just prior to the peak stress (Torreti et al., 1993). For this reason compressive failure is suitable to be analyzed by means of Fracture Mechanics (Van Mier, 1984).

Some recent experimental works based on Fracture Mechanics to study the compressive behavior of concrete are especially noteworthy. Jansen and Shah (Jansen and Shah, 1997) planned an experimental program aimed at analyzing the effect of the specimen slenderness on the compressive strength. Also notable is the work by Choi et al. (Choi et al., 1996), on the strain softening in compression under different end constraints. Borges et al. (Borges et al., 2004) studied the ductility of concrete in uniaxial and flexural compression. The results of these experimental programs suggest that the compressive test may be considered as an structural test, because the results depend not only on the actual mechanical properties but on the geometry of the specimen and on the boundary conditions, like end constraints, feedback signal or specimen capping (Shah et al., 1995).

In the last decades concrete technology has made it easier to reach higher strengths and the so-called High-Strength Concrete (HSC) has appeared as a new construction material. This amount of the compressive strength provokes that the normalized specimens for normal strength concrete, e.g. 150×300mm cylinder (diameter $\times$ height), may surpass the capacity of standard laboratory equipment. To overcome this drawback HSC mixtures are often evaluated using 100×200mm cylinders, which also meet the requirements of ASTM C39. The strength obtained with this specimen is higher in average than that obtained with 150×300mm cylinders. This size effect on the compressive strength manifests that the specimen is not behaving as simply as it may look. Indeed, size effect is understood as the dependence of the nominal strength of a structure on its size (dimension) when compared to another geometrically similar structure (Bažant and Planas, 1998). For quasi-brittle materials
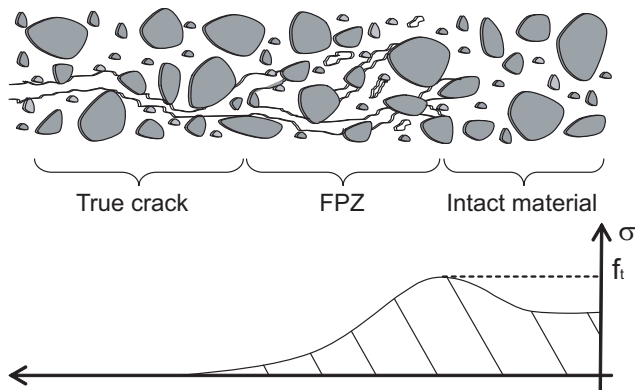
Figure 1: Fracture process zone (FPZ).

Dimensions in mm.

Figure 2: Specimen geometry.

as concrete, the presence of a non-negligible fracture process zone at the front of the crack, which is commensurate with an internal characteristic length and with the typical size of the material inhomogeneities, provokes a deterministic size effect (please, see Figure 1).

In this paper we investigate the mechanical behavior of HSC (around 100 MPa) tested in a compressive setup in axial strain control. We are particularly interested in the influence of the shape and of the size of the specimens on the compressive strength, f_c, of the material. According to our results we propose a new relationship between cylinder and cube specimens.

The article is organized as follows. An outline of the experimental program is given in Section 2. Concrete production and specimens are described in Section 3. In Section 4 we describe the testing procedures. The experimental results are presented and discussed in Section 5. Section 6 includes a simple analysis of size effect and establishes a relationship between the compressive strength measured from standard cylinders and the one obtained from cubes of different sizes. Finally, in Section 7 some conclusions are extracted.

2 OVERVIEW OF THE EXPERIMENTAL PROGRAM

The experimental program was designed to study the size and shape effect on compressive tests performed on High-Strength Concrete (HSC) specimens. Specifically, we wanted to disclose the influence of the size in cubes and the relationship between compressive strength obtained from standard cylinders, ASTM C39 (100×200mm) and the strength got from cubes. We also intended to analyze the variations in the crack pattern and in the mechanical behavior due to the size and shape of the specimens.

With these intentions in mind, we chose the specimens sketched in Figure 2. We use cylinders and cubes of different sizes: the dimensions of the cylinders are 75×150 and 100×200mm (diameter $\times$ height); the edges of the cubes are 33, 50, 67
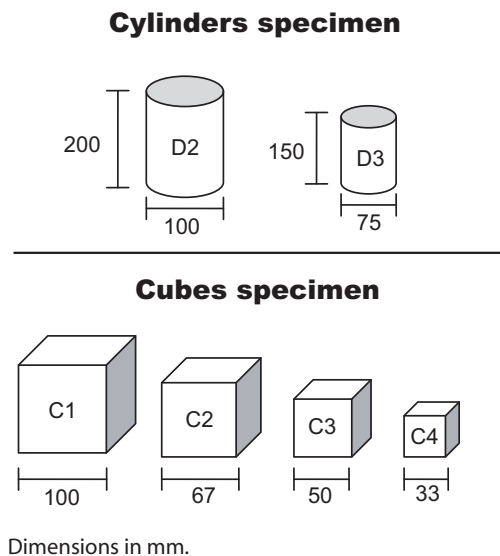
and 100 mm long. The dimensions of the cylinders were scaled to the diameter D, while the dimensions of the cylinders were scaled to the edge L, please see Figure 2. Each specimen was named by a letter indicating the shape, D for cylinders and C for cubes, and one number which indicates the size. For example, D2 names a cylinder of 100×200mm. We performed at least four tests for each type of specimen.

An important feature of our experimental program —unlike most of the tests available in the scientific literature— consists of providing complete material characterization obtained by independent tests, in many cases performed according to Standard recommendations. Specifically, we measured the compressive strength, the tensile strength, the elastic modulus and the fracture energy of the concrete.

3 MATERIAL AND SPECIMENS

A single high-strength concrete mix was used throughout the experimental program. It was made with a andesite aggregate of 12mm maximum size and ASTM type I cement. Microsilica fume slurry and superplasticizer (B-255, BASF) were used in the concrete composition. The water to cement ratio (w/c) was fixed to 0.28.

There was a strict control of the specimen-making process, to minimize scatter in test results. In the case of cylinders the concrete was poured into steel molds in three layers and compacted on a vibration table. In the case of the cubes the specimens were taken by wet-sawing from $100 \times 100 \times 420$mm concrete prisms. The prisms were also made using steel molds and a vibration table. Cylinders and prisms were wrap-cured for 24 hours, demolded and stored in a moist chamber at 20ºC and 96% relative humidity. Right after making the cubes from the prisms their sides, as well as the bases of the cylinders, were surface-ground with a wet diamond wheel to en-

Table 1: High strength concrete mechanical properties.

| | f_c [a] | f_{ts} [b] | E_c | G_F | ℓ_{ch} [c] |
	MPa	MPa	GPa	N/m	mm
mean	89.6	5.4	36.1	119.0	147.3
std. dev.	7.13	0.6	1.1	13.5	-

[a] Cylinder, compression tests, D2.

[b] Cylinder, splitting tests.

[c] $\ell_{ch} = \frac{E_c G_F}{f_t^2}$

sure perfectly-plane and parallel surfaces. Of course, the specimens were immediately stored again in the chamber until testing time (six months from concrete making). Just before testing the length, diameter and weight of the cylinders and the height and weight of cubes were measured.

Table 1 shows the characteristic mechanical parameters of the micro-concrete determined in the various characterization tests. In the table it is also shown the characteristic length of the concrete, ℓ_{ch}, (Petersson, 1981), which is defined as $\ell_{ch} = E_c G_F / f_t^2$, being E_c the elastic modulus, G_F the fracture energy and f_t the tensile strength. Please, notice that the characteristic length, ℓ_{ch}, of this concrete is roughly 150 mm, closely half the ℓ_{ch} of normal concrete (ℓ_{ch}=300mm). This means that, from a Fracture Mechanics standpoint, we expect that high-strength concrete (HSC) may present a more brittle behavior than NSC for the same specimen size. As mentioned above, the characteristic length is related with the extension of the fracture processes zone (FPZ), see Figure 1.

4 EXPERIMENTAL PROCEDURES

4.1 *Characterization tests*

Compressive tests were carried out on 4 cylindrical specimens according to ASTM C-39 on 100×200mm (diameter $\times$ height), except for a reduction of the axial displacement rate of the machine actuator, which was 0.018mm/min.

The Elastic modulus was obtained according to ASTM C-469 on cylindrical specimens of 150×300mm. The strain was measured over a 50mm gage length by means of two inductive extensometer placed symmetrically, on a similar setup that it is shown in Figure 3. The tests were run under displacement control, at a rate of 0.3mm/min.

Brazilian tests were also carried out on cylindrical specimens following the procedures recommended by ASTM C496 on 150×300mm cylinders (diameter $\times$ height). The specimen was loaded through plywood strips with a width of 1/6 of the specimen diameter. The velocity of displacement of the machine actuator was 0.18mm/min.
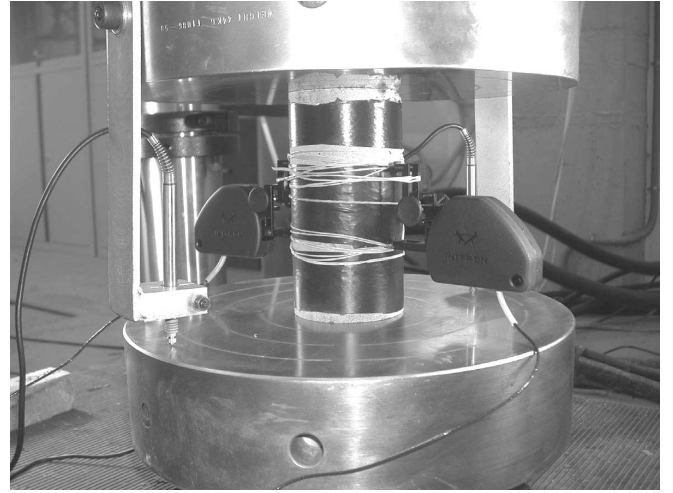
Stable three-point bend tests on

Figure 3: Testing setup for D3 specimen.

$100 \times 100 \times 420$mm notched beams were carried out to obtain the fracture properties of concrete following the procedures devised by Elices, Guinea and Planas (Guinea et al., 1992; Elices et al., 1992; Planas et al., 1992). During the tests the beams rested on two rigid-steel semi-cylinders laid on two supports permitting rotation out of the plane of the beam and rolling along the beam's longitudinal axis with negligible friction. These supports roll on the upper face of a very stiff steel beam fastened to the machine actuator.

Table 1 shows the characteristic mechanical parameters of the micro-concrete determined in the various characterization tests.

4.2 *Testing procedure to obtain stable σ-ε curves*

All the specimens were tested on a compressive setup as illustrated in Figure 3. The experiments were performed on an INSTRON 8800 closed-loop servo-hydraulic dynamic testing machine, with a capacity of 1000kN. The loading platens are made of hardened steel and have polished surfaces. Two linear variable differential transformers (LVDTs), having a calibrated range of ±2.5mm, were placed opposed to the specimen in a symmetric fashion. These LVDTs were used to measure axial platen-to-platen displacement, δ. The axial deformation referred to in this paper is the average value of the two LVDTs.

For controlling the tests, the signal of the average axial displacement from the LVDTs was chosen. This average signal represents the axial displacement velocity at the center of the loading platen. This type of control leads to stable tests for our particular material and specimens geometry. The axial strain rate is defined as $\dot{\varepsilon} = \dot{\delta}/L$, where $\dot{\delta}$ is the axial platen-to-platen displacement rate and L is the initial distance between the top and bottom plane surfaces over the height of the specimen. This axial strain rate was kept constant for all tests having a value of $10^{-6}s^{-1}$. The axial displacement rates selected for each specimen

Table 2: Axial displacement rate for each of the specimens.

Denomination	Axial displacement rate, $\dot{\delta}$ mm $\times$ min^{-1}
D2	1.8×10^{-2}
D3	1.2×10^{-2}
C1	0.9×10^{-2}
C2	0.6×10^{-2}
C3	0.4×10^{-2}
C4	1.98×10^{-3}

are showed in Table 2.

An elastic band was stuck around the specimen, see Figure 3, (1) to preserve the fragments together for a posterior analysis, and (2) to avoid a interchange of humidity with the environment during the test. The transversal force provoked by this elastic band is negligible.

The load, P, and the axial displacement, δ, were continually monitored and recorded. We used a pair of clip extensometer centered on the specimen in D2 and D3 to measure the displacement in the central part of the specimen in order to get the elastic modulus. To complete the experimental information, we also took pictures of the crack pattern resulting from each test.

5 RESULTS AND DISCUSSION

The discussion of the results is organized as follows. First we present and describe the $\sigma - \varepsilon$ curves obtained from the tests. Then we proceed to discuss size effect in cubes and cylinders. Finally the crack patterns are analyzed. Let us emphasize again that cylinders and cubes were tested in strain control keeping

Table 3: Strength and strain at peak and ultimate load.

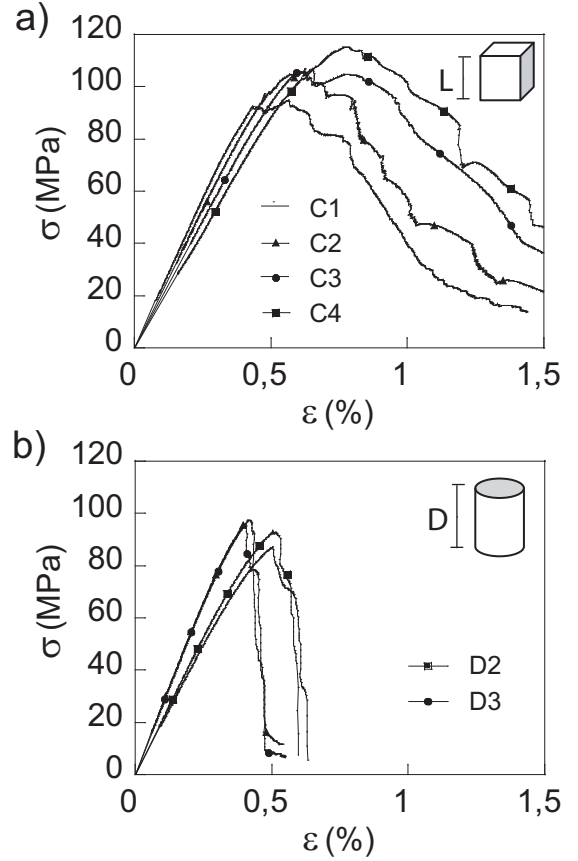| Specimen		σ_c MPa	ϵ_c %	σ_u MPa	ε_u %
D2	mean	89.6	0.37	31.4	0.71
	desv. std.	7.11	0.02	23.31	0.51
D3	mean	89.9	0.34	41.6	0.22
	desv. std.	4.65	0.02	22.08	0.42
C1	mean	96.1	0.57	12.7	1.53
	desv. std.	1.63	0.01	1.55	0.12
C2	mean	102.4	0.61	20.9	1.59
	desv. std.	9.93	0.03	1.81	0.19
C3	mean	104.2	0.66	38.5	1.46
	desv. std.	2.19	0.06	6.63	0.13
C4	mean	110.0	0.85	33.8	1.94
	desv. std.	7.34	0.09	5.09	0.35

Figure 4: $\sigma - \varepsilon$ Curves corresponding to: (a) Cubes; (b) Cylinders.

constant the axial strain rate throughout the experimental program.

5.1 $\sigma - \varepsilon$ curves

Table 3 lists the average value and the standard deviation for the peak stresses, σ_c, the strain at peak stress, ε_c, the ultimate stress recorded, σ_u, and the ultimate strain recorded, ε_u for all specimens. As expected, σ_c increases noticeably as the size of the specimen decreases. The strain at peak load increases also as size decreases.

Figure 4a and 4b compare $\sigma - \varepsilon$ curves for selected sizes. Specifically, Figure 4a shows the $\sigma - \varepsilon$ obtained for cubes and Figure 4b for cylinders. The x-axis corresponds to the average strain, i.e. the displacement between the top and bottom plane surfaces over the height of the specimen. The y-axis corresponds to the concrete stress ($\sigma_c = \frac{P}{Area}$). A typical $\sigma - \varepsilon$ curve starts with a linear ramp-up. The initial slope shows no significant variations due to the size in the case of cubes while in cylinders the shorter specimen shows a higher slope. In both cases there is a loss of linearity before reaching the peak load, which indicates the initiation of fracture processes.

The post peak behavior depends on the specimen shape. In the case of cylinders, Figure 4b, a sudden drop in the load takes place after the peak load and no significant changes are reported in the softening
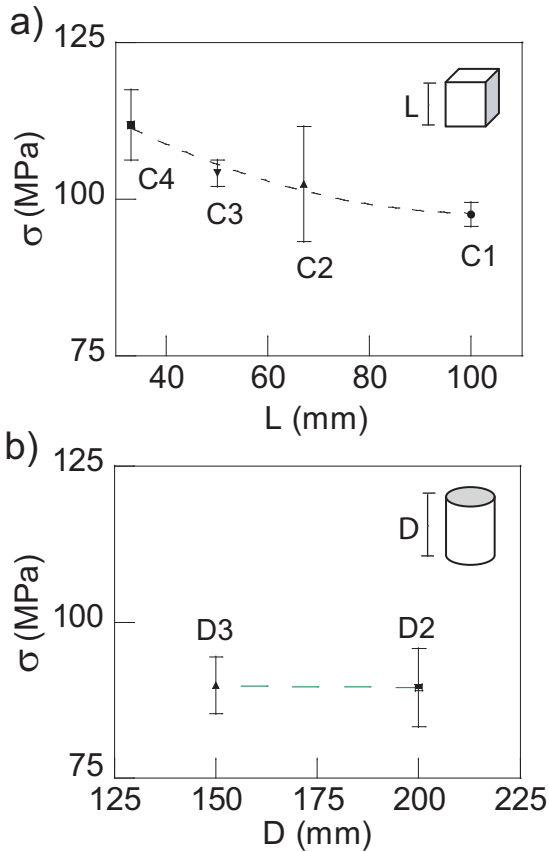
Figure 5: Size effect on the peak strength: (a) Cubes; (b) Cylinders.

Figure 6: Crack pattern for: (a) Cubes; (b) Cylinders.

branch between the scaled tested cylinders. In the case of cubes, Figure 4a, $\sigma - \varepsilon$ curves show a not so steep softening branch which is associated to a milder failure localization and to a large amount of volumetric energy dissipation, in contrast with the strong failure localization observed in cylinders.

5.2 Size effect

Figures 5a and b plot the peak loads or maximum strength obtained in the $\sigma - \varepsilon$ curves for the different tested specimens, against a characteristic dimension of the specimen. In Figure 4a is drawn the case of cubes specimens. It is clearly observed that large specimens resist less in terms of stress than the smaller ones. A interpolation line has been plotted attached to the tests results to facilitate the comparison. Size effect is less noticeable as size increases.

By contrast, the average stress, σ, obtained from cylinders is roughly constant within the experimental size interval planned for this research and approximately 10% lower than the horizontal asymptote for the cubes as it can be observed in Figure 4b.

5.3 Crack pattern

The crack pattern observed after the test is sensitive to the shape of the specimen as Figure 6 shows. The extent of micro-cracking throughout the specimen is denser in the cubes t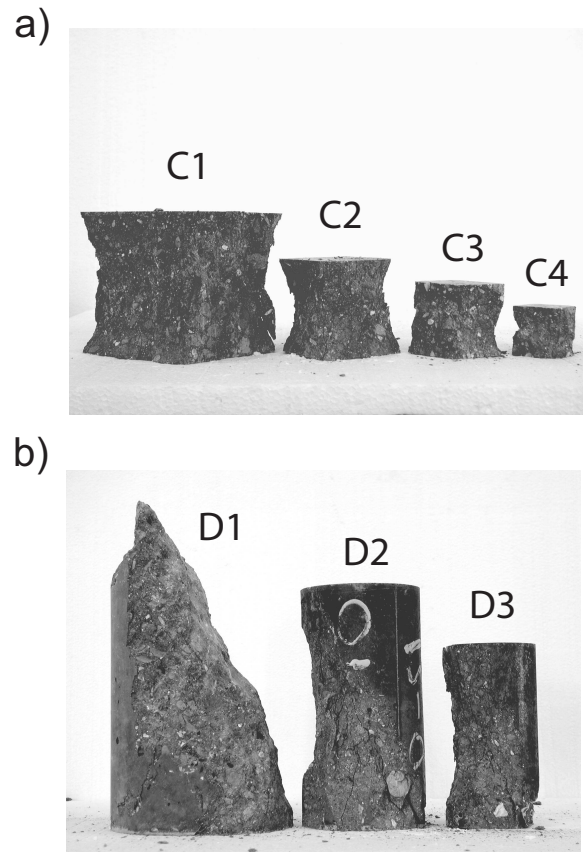han in the cylinders. Indeed, a main inclined fracture surface is nucleated in cylinders, whereas in cubes we find that the lateral sides get spalled and that there is a dense columnar cracking in the bulk of the specimen. This is consistent with the observation made in Section 5.1 about the differences in the $\sigma - \varepsilon$ curves between cubes and cylinders. The steeper response observed in the $\sigma - \varepsilon$ curves for cylinders may be associated to the inclined fracture surface or cone type failure, see Figure 6b, with a initial localization failure in the central part of the specimen. In the case of cubes the fracture process is provoked by a stress concentration near the cube corners. Inclined micro-cracks appear and coalesce near the corners and provoke the crack pattern observed. The stress state inside the cubes provokes vertical cracks that en-up forming column-like fragments. The extent of the micro-cracking in this fracture process leads to a higher energy consumption than in the case of cylinders.

Another interesting point is that the failure pattern observed is almost independent for scaled elements in the size interval planned for the experimental program. Cylinders broke in all cases by a diagonal fracture plane and cubes present a bursting rupture combined with a dense columnar cracking. We have also included the crack pattern obtained for a cylinder of 150×300mm, called D1, in Figure 6b.

6 RELATIONSHIP BETWEEN CYLINDER AND CUBE STRENGTH BASED ON FRACTURE MECHANICS THEORIES

In this section we analyze the test results showed in section 5 within a Fracture Mechanics frame. The aim of this analysis is to get a relationship between cylinder and cube strength. According to Bazant and Planas (Bažant and Planas, 1998) the maximum load P_c is a function of the specimen geometry (shape and size), boundary conditions and concrete properties. In this investigation only the size and shape are varied, keeping constant the boundary conditions. For the sake of simplicity, the nominal strength at peak load, σ_N, for a concrete specimen is represented by the generalized deterministic energy-based formula for size effect at crack initiation proposed by Bažant (Bažant, 1998). Its applicability is based on the fact the failure is provoked by crack initiation, which is our case as shown in the previous section. So, we can write σ_N as:

$$\sigma_N = \sigma_\infty \Big(1 + \frac{B}{\beta_H}\Big)^{\frac{1}{r}} \tag{1}$$

$$\sigma_\infty = \kappa \sigma_0$$

where σ_∞ is the theoretical strength for a specimen of a infinite size and σ_0 is a reference strength, which in our case we take as the strength that is obtained from the standard test (ASTM C-39 on 100×200mm cylinders). B and κ are empirical constants dependent on the specimen shape and fracture properties of the material, but not on the structural size. Both constants can be obtained from test results. β_H is the denominated Hillerborg's brittleness number (Bažant and Planas, 1998). It is defined as the ratio between the representative size of the specimen —represented by the depth D in the case of cylinders, and L in the case of cubes— and the characteristic length of the concrete. The values of the exponent r using in concrete ranges from 1 to 2 (Bažant, 1998). The formulation when the exponent r is equal to 2, is identical to the formula proposed on the basis of strictly geometric arguments proposed by Carpinteri and coworkers (Carpinteri et al., 1998). The size effect law can be rewritten as:

$$\sigma_N = \sigma_\infty \sqrt{1 + \frac{B}{\beta_H}} \tag{2}$$

Applicability of Eqs. 1 and 2 requires not only that the specimens are scaled to each other, but also that the shape of cracks patterns must be similar. In our case the crack patterns for cubes are very similar, as we showed in Section 5.3.

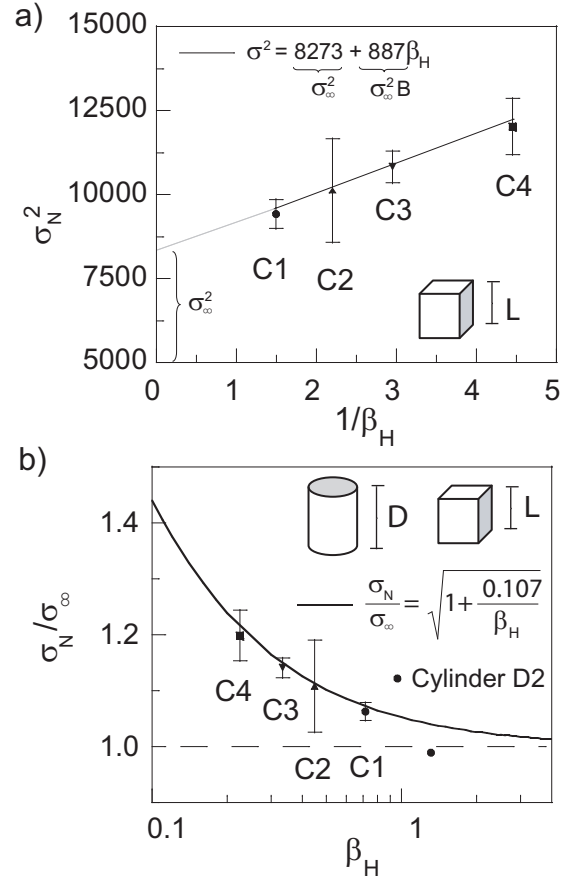Figure 7a shows the linear regression made with the cubes to get the constants κ and B. Please note that

Figure 7: Size effect in the peak load: (a) Results for the regression to calibrate σ_∞ and B coefficients for cubes specimens; (b) Size effect law.

the Pearson's correlation coefficient, R in Figure 7a is close to 1. Figure 7b show the test results compared to the obtained size effect law in a non-dimensional fashion. It may be pointed out that size effect tends to disappear when $D \to \infty$. The compressive strength converges to a value that in our case is quite similar to 1, that is, for big sizes the compressive strength in cubes converges to the compressive strength obtained with the standard procedure. Further analysis would be necessary to evaluate the influence of the displacement control platen-to-platen velocity. The strength for a specimen of infinite size can be evaluated as $\sigma_\infty = \sigma_0 \kappa$. In our case σ_∞ is equal to 88.7 MPa.

Based on the obtained law a correlation between compressive strength obtained for different cubes specimens, σ_{cub}, and for Standard tests, f_c, can be derived. In a general way for concrete which compression standard is around 100MPa and have a characteristic length of 150 mm, the next simplified relationship arises. For HSC like the one used in this research $f_c = \sigma_0 \approx 100$MPa, $\ell_{ch} \approx 150$mm and $\sigma_{cub} = \sigma_N$, the expression is:

$$f_c = \sigma_{cub} \sqrt{\frac{L}{L + L_0}} \tag{3}$$

where L is the side of the cube and L_0 is a empiri-

cal constant equal to 20mm in this case. The fact that cubes are somewhat easier to test, since cubes provide directly two couples of perfectly-plane parallel surfaces and they not require capping, together with the necessity of using specimens whose strength do not surpass the capacity of standard equipment, suggest that cubes would be a solution for compressive test characterization. The tendency to prefer cylinder to cubes, in our opinion does not have a solid foundation due to the structural character of the compressive test. There is not a reason to think that cylinders catch concrete compressive behavior better than cubes, since compressive tests depend strongly on many factors other than the actual material properties. The standard compressive strength of HSC could be obtained from cubes using the simplified expression showed in Eq. 3.

With this example we want to show how that using Fracture Mechanics theories provide solutions for concrete technological problems. These solutions may help to understand concrete behavior and structural failures better.

7 CONCLUSIONS

In this paper we investigate the mechanical behavior of high-strength concrete (around 100 MPa) in compression and tested in strain-control. We are particularly interested in the influence of the shape and the size of the specimens on the compressive strength, f_c, of the material. Cylinders and cubes were tested in strain control at a rate that was kept constant throughout the experimental program. Concrete making and testing procedures were closely controlled to reduce experimental scatter. The following conclusions can be drawn from the study:

1. The prepeak and post-peak behavior in the $\sigma - \varepsilon$ curves are dependent on the specimen size and shape. Cubes show a mild failure localization in contrast with the strong failure localization observed in cylinders.

2. Test results show size effect. Large specimens resist less in terms of stress than the small ones. The size effect in the cubes is quite stronger than in cylinders, where the average strength obtained is roughly constant within the size interval planned for this research.

3. The crack pattern observed after the test is sensitive to the shape of the specimen. A main inclined fracture surface is nucleated in cylinders, whereas in cubes we find that the lateral sides get spalled and that there is a dense columnar cracking in the bulk of the specimen. This is consistent with the differences observed in the $\sigma - \varepsilon$ curves

between cubes and cylinders. Interestingly, the failure pattern does not change with the size.

4. The size effect in the compressive strength of cubes is described by a simple model based on Fracture Mechanics concepts. A relationship between standard cylinder strength and strength obtained from cubes of any size is derived. It discloses the influence of the cube dimension and may help to deduce relations between the compressive strength determined from cylinders and cubes, inside a theoretical Fracture Mechanics frame.

REFERENCES

Bažant, Z. P. (1998). Size effect in tensile and compression fracture of concrete structures: Computational modeling and desing. In *Fracture Mechanics of Concrete Structures*, pages 1905–1922, Freiburg, Germany. F.H. Wittmann, Ed., Aedificatio Publishers.

Bažant, Z. P. and Planas, J. (1998). *Fracture Size Effect in Concrete and Other Quasibrittle Materials*. CRC Press, Boca Raton.

Borges, J. U. A., Subramaniam, K. V., Weiss, W. J., Shah, S. P., and Bittencourt, T. (2004). Length effect on ductility of concrete in uniaxial and flexural compression. *ACI Structural Journal*, 101(6):765–772.

Carpinteri, A., Chiaia, B., and Ferro, G. (1998). Size effect on nominal tensile strength of concrete structures: Multifractality of material ligaments and dimensional transition from order to disorder. *Materials and Structures*, 28:311–317.

Choi, S., Thienel, K. C., and Shah, S. P. (1996). Strain softening of concrete in compression under different end constraints. *Magazine of Concrete Reseach*, 48(175):103–115.

Elices, M., Guinea, G. V., and Planas, J. (1992). Measurement of the fracture energy using three-point bend tests. 3. Influence of the cutting the $P - \delta$ tail. *Materials and Structures*, 25:327–334.

Guinea, G. V., Planas, J., and Elices, M. (1992). Measurement of the fracture energy using three-point

bend tests. 1. Influence of experimental procedures. *Materials and Structures*, 25:121–128.

Jansen, D. C. and Shah, S. P. (1997). Effect on length on compressive strain softening of concrete. *Journal of Engineering Mechanics-ASCE*, 123(1):25–35.

Mindess, S., Young, J. F., and Darwin, D. (2003). *Concrete*. Prentice Hall, Pearson Education, Inc. United States of America.

Petersson, P. E. (1981). *Crack Growth and Development of Fracture Zones in Plain Concrete and Similar Materials*. Report No. TVBM-1006, Division of Building Materials, Lund Institute of Technology, Lund, Sweden.

Planas, J., Elices, M., and Guinea, G. V. (1992). Measurement of the fracture energy using three-point bend tests. 2. Influence of bulk energy dissipation. *Materials and Structures*, 25:305–312.

Shah, S. P. and Sankar, R. (1987). Internal cracking and strain-softening response of concrete under uniaxial compression. *ACI Materials Journal*, 84(3):200–212.

Shah, S. P., Swartz, S. E., and Ouyang, C. (1995). *Fracture Mechanics of Concrete*. Wiley, New York.

Torreti, J. M., Benaija, E. H., and Boulay, C. (1993). Influence of boundary conditions on strain softening in concrete compression tests. *Journal of Engineering Mechanics-ASCE*, 119(12):2369–2384.

Van Mier, J. G. M. (1984). *Strain-softening of concrete under multiaxial loading conditions*. PhD thesis, Eindhoven University of Technology, Eindhoven, The Netherlands.